University of Dayton
eCommons

Chemical and Materials Engineering Faculty Publications | Department of Chemical and Materials Engineering

2014

Thermal Anisotropy in Nano-Crystalline MoS2 Thin Films

Christopher Muratore
University of Dayton, cmuratore1@udayton.edu

Vikas Varshney
Air Force Research Laboratory

Jaime J. Gengler
Air Force Research Laboratory

Jianjun Hu
University of Dayton, jhu001@udayton.edu

John E. Bultman
University of Dayton, jbultman1@udayton.edu

See next page for additional authors

Follow this and additional works at: https://ecommons.udayton.edu/cme_fac_pub

Part of the Other Chemical Engineering Commons, Other Materials Science and Engineering Commons, and the Polymer and Organic Materials Commons

eCommons Citation
Muratore, Christopher; Varshney, Vikas; Gengler, Jaime J.; Hu, Jianjun; Bultman, John E.; Roy, Ajit K.; Farmer, Barry L.; and Voevodin, Andrey A., "Thermal Anisotropy in Nano-Crystalline MoS2 Thin Films" (2014). *Chemical and Materials Engineering Faculty Publications*. 101.
https://ecommons.udayton.edu/cme_fac_pub/101

This Article is brought to you for free and open access by the Department of Chemical and Materials Engineering at eCommons. It has been accepted for inclusion in Chemical and Materials Engineering Faculty Publications by an authorized administrator of eCommons. For more information, please contact frice1@udayton.edu, mschlangen1@udayton.edu.

Author(s)
Christopher Muratore, Vikas Varshney, Jaime J. Gengler, Jianjun Hu, John E. Bultman, Ajit K. Roy, Barry L. Farmer, and Andrey A. Voevodin

This article is available at eCommons: https://ecommons.udayton.edu/cme_fac_pub/101

PCCP

PAPER

View Article Online
View Journal | View Issue

Thermal anisotropy in nano-crystalline MoS_2 thin films

Cite this: *Phys. Chem. Chem. Phys.*, 2014, **16**, 1008

Chris Muratore,†*[ab] Vikas Varshney,†[bc] Jamie J. Gengler,[bd] Jianjun Hu,[be] John E. Bultman,[be] Ajit K. Roy,[b] Barry L. Farmer[b] and Andrey A. Voevodin[b]

Received 4th September 2013,
Accepted 13th November 2013

DOI: 10.1039/c3cp53746c

www.rsc.org/pccp

In this work, we grow thin MoS_2 films (50–150 nm) uniformly over large areas (>1 cm^2) with strong basal plane (002) or edge plane (100) orientations to characterize thermal anisotropy. Measurement results are correlated with molecular dynamics simulations of thermal transport for perfect and defective MoS_2 crystals. The correlation between predicted (simulations) and measured (experimental) thermal conductivity are attributed to factors such as crystalline domain orientation and size, thereby demonstrating the importance of thermal boundary scattering in limiting thermal conductivity in nano-crystalline MoS_2 thin films. Furthermore, we demonstrate that the cross-plane thermal conductivity of the films is strongly impacted by exposure to ambient humidity.

Introduction

Transition metal dichalcogenides (TMDs) are a re-emerging class of layered materials, which have been a focus of extensive research for diverse applications including solid lubrication,[1] catalysis,[2] and most recently, as potential semiconducting materials[3] for 2D nanoelectronic devices. Within the latter scope, it is well known that thermal properties of semiconducting TMD materials are closely coupled with their electronic properties, and ultimately, with device performance.[4] Extreme thermal gradients can limit operational efficiency and reliability for switching or signal amplification. Thus, a better understanding of thermal properties of 2D semiconducting materials should enable the design and practical use of a host of new devices recently suggested in the literature,[5,6] with enhanced performance and lifetime.

TMDs are often characterized by 'MX_2' type of 2D hexagonally arranged atomic structure where M corresponds to a transition metal (often Mo and W) while X is a chalcogen (such as S, Se, or Te). Because of their inherent 2D layered structure, these materials demonstrate significant anisotropy of in-plane (*i.e.*, basal plane) *vs.* out-of-plane (*i.e.*, cross-plane) physical properties due to differences in the nature of the atomic interactions along the two directions. Within a molecular layer (in-plane), these interactions are characterized by covalent bonding, while the individual layers (cross-plane) are held together by significantly weaker van der Waals forces. Such structural arrangements are in principle similar to graphene and potentially provide significant in-plane electron mobilities (>500 cm^2 V^{-1} s^{-1}),[7] while providing one particular advantage over the graphene for electronics – an intrinsic band gap, which can be as large as 1.9 eV for monolayer MoS_2.[3] The unique electronic transport properties coupled with the potential for strain-free heterostructures due to van der Waals bonding at layer interfaces have ignited a great deal of motivation to explore TMDs as a class of 2D materials beyond graphene in diverse research areas, such as sensing,[8] energy harvesting,[9] and flexible electronics.[10] To realize many of these applications, a better understanding of thermal transport in TMD structures is needed.

The focus of the research presented here is an investigation of the thermal transport properties of molybdenum disulfide (MoS_2) thin films. While the effects of the aforementioned bonding anisotropy on many properties of MoS_2 are well-known, its thermal properties have only been investigated recently.[11,12] Moreover, unlike well-studied properties of electrically conductive graphite and insulating hexagonal boron nitride in bulk[13–15] and few-layer[16,17] forms, the few published reports on thermal properties of TMD materials have been focused on the cross-plane direction, often highlighting the extremely low values for thermal conductivity. For example, thin, turbostratic films of WSe_2 (tungsten diselenide) have been shown to have the lowest cross-plane thermal conductivity of any fully dense material.[11,18] These materials with a high degree of atomic order were demonstrated to have thermal conductivity values lower than their amorphous counterparts, and an order of magnitude lower conductivity than bulk crystals

[a] *Department of Chemical and Materials Engineering, University of Dayton, Dayton, OH 45469, USA. E-mail: cmuratore1@udayton.edu*
[b] *Materials and Manufacturing Directorate, Air Force Research Laboratory, Wright-Patterson Air Force Base, OH 45433, USA. E-mail: vikas.varshney@wpafb.af.mil*
[c] *Universal Technology Corporation, Dayton, OH 45432, USA*
[d] *Spectral Energies LLC, 5100 Springfield Street, Suite 301, Dayton, OH 45431, USA*
[e] *University of Dayton Research Institute, 300 College Park, Dayton, OH 45469, USA*
† Both authors contributed equally to this work.

This journal is © the Owner Societies 2014

of the same composition due to phonon scattering at domain boundaries within the material. As scalable TMD growth techniques are adopted for device fabrication with 2D materials, the role of domain boundaries and other atomic-scale defects on electron and phonon scattering is anticipated to make a significant contribution to device performance and operation. As our understanding of the thermal properties of graphene has benefited from the rigorous understanding of phonon transport in graphite, we aim to understand the thermal properties of bulk and nanocrystalline thin MoS_2 films to aid in the design of mono- and few-layer TMD devices.

Due to the semiconducting nature of bulk MoS_2 crystals (1.2 eV band gap for >4 molecular layers of MoS_2[3]), atomic vibrations (phonons) are expected to dictate its thermal conduction behavior. Moreover, some degree of thermal anisotropy is also anticipated, primarily due to the differences in phonon propagation characteristics along the covalently bonded basal plane and across weakly interacting basal planes. Each basal plane could be considered to possess an interface in the form of a van der Waals gap every three atomic layers (*i.e.* at every S–Mo–S/S–Mo–S interface) resulting in phonon localization.[18] While the thermal anisotropy (in-plane *vs.* out-of-plane conduction) is reported to be as high as a factor of 200 for pristine graphite, a more moderate value of $\sim$30 was observed for WSe_2 (TMD) thin films, grown by the modulated elemental reactants technique[19] and characterized with the 3ω technique.[20] This reduction in the magnitude of in-plane *vs.* cross-plane anisotropy as compared to graphite can be attributed to differences between in-plane bond strength, cross-plane interactions, and atomic mass between molecular layered materials (as in TMDs) and atomic layered materials (as in graphite).

Here, we report on the thermal conductivity of strongly (002) and (100) oriented MoS_2 thin films of $\sim$70–250 molecular layers (50–150 nm thickness) grown *via* sputter deposition, along with that of a bulk MoS_2 sample from a geological specimen. We use the time domain thermo-reflectance (TDTR) technique for measurement of the thermal conductivity of MoS_2 films as well as the bulk geo-specimen sample, and investigate the physical mechanisms resulting in the observed thermal anisotropy. We also use molecular dynamics (MD) simulations to investigate the origins of our measurement results by incorporating different domain boundary densities into the MoS_2 films by altering the domain size and correlating boundary scattering phenomena to predicted in-plane and out-of-plane thermal conductivity values.

Experimental section

Thin film growth

Thin films were sputtered from a pure (>99.9%) MoS_2 target in an ultra-high vacuum growth chamber with a base pressure of $<5 \times 10^{-9}$ Torr. The power to the sputter target was modulated *via* an Advanced Energy Pinnacle Plus power supply. By altering the frequency and duration (dictated by the 'reverse' or off time) of the nominal power applied to the sputter target, the orientation of the films was adjusted similar to the methods reported in ref. 21. The deposited films ranged in thickness between 50–150 nm. The substrates were polished, polycrystalline Inconel 718 nickel superalloy disks (2.5 cm) that were electrically grounded and heated to 300 °C prior to film growth for degassing, and maintained at that temperature during film growth (except for an amorphous MoS_2 sample which was grown at room temperature). Film composition was characterized with an *in vacuo* X-ray photoelectron spectroscopy (XPS) system in line with the processing chamber allowing analysis of the films after growth but prior to exposure to the ambient atmosphere. In such cases, no oxygen was detected, and the films appeared to be stoichiometric within the compositional resolution of the system which was approximately 2 atomic percent. A set of MoS_2 films deposited under identical conditions was immediately coated with a 70 nm layer of aluminum (Al) also without breaking vacuum to avoid atmospheric exposure of the film surfaces. The aluminum overcoat was used as a thermal transducer in TDTR experiments and also served as a protective layer during transmission electron microscopy (TEM) sample preparation of the films *via* focused ion beam. In a related experiment, sets of MoS_2 films were stored in laboratory air ($\sim$35% relative humidity) for 48 hours before coating with Al to investigate the effect of oxygen ingress on the film composition and thermal conductivity modifications (discussed later).

The samples were characterized using X-ray diffraction in a Bragg–Brentano configuration to evaluate the overall film orientation, as the X-rays penetrated the thickness of the MoS_2 films and into the substrates. This is especially useful for characterization of materials such as MoS_2 which often demonstrate a change in crystalline orientation from (002) to (100) throughout their thickness due to the dynamic growth kinetics as reported previously.[22]

Thermal conductivity characterization

The thermal conductivity of the deposited films was measured using the TDTR technique. This is an ultra-fast laser-based approach for measuring thermal properties of materials by monitoring time-resolved, temperature-induced changes in optical reflectivity synchronized to delivery of an infrared laser heating pulse delivered to the material surface which has been described in detail elsewhere.[23,24] Due to the substantial aspect ratio of laser pulse spot size to thermal penetration depth, the TDTR measurements are selectively sensitive to one-dimensional thermal transport properties perpendicular to the sample surface (*i.e.* in the cross-plane direction for (002) deposited MoS_2 sample). This is due to the high modulation frequency of 9.8 MHz, coupled with the relatively low thermal conductivity of MoS_2. For analysis in our studies, we included the thermal and physical property data of the Inconel substrate from ref. 25 when modeling the TDTR data. It was found that the lower limit for film thickness at which we could reliably measure thermal conductivity for MoS_2 and other TMD materials with the TDTR technique is around 50 nm,[11] as data from thinner samples was difficult to fit based on the model we used for analysis. However, thermal interface conductance could, in principle, be measured for interfaces involving much thinner films ($\sim$1 nm), providing they are

grown uniformly over an area comparable to the beam diameter (∼50 microns in our experiments). Thermal conductivity of MoS_2 samples coated with Al prior to and after controlled exposure to the ambient atmosphere, were measured, along with a bulk MoS_2 geospecimen sample with (002) orientation that was freshly cleaved in air immediately prior to Al coating.

Modeling section

Previously, we successfully parameterized a classical force-field and modeled thermal conduction in pristine MoS_2 crystals along in-plane and cross-plane directions[26] using MD simulations. The force-field was parameterized with respect to experimental crystal structure and vibrational spectra measurements of MoS_2. In the current work, we extend the MD simulation approach to investigate the effect of domain boundaries observed in sputtered TMD thin films[11] and understand their impact on thermal conductivity. For this purpose, a simplistic model of in-plane crystalline domains with edge defects was generated and was modeled using MD simulations as discussed below.

Model preparation

First, a periodic pristine long slab of MoS_2 was created with dimensions of 78 nm × 2.3 nm × 2.5 nm, which corresponded to 240, 8, and 2 repeat units of primitive unit-cell along *X*-, *Y*- and *Z*-direction (Fig. 1c). Within this slab, a pre-defined number ($2n$) of edges along basal planes (to model crystalline domains) were introduced by deleting in-plane bonds across n planes to create sharp interfaces along the basal plane direction within the crystal. In doing so, the deletion of n = 1, 2, 3, 4, 6, and 20 planes resulted in crystalline domains with parallel orientation of size 39, 26, 19.5, 15.6, 11, and 3.75 nm, respectively (Fig. 1c). In addition, we should point out that each of these domains were of identical length along the crystal. A representative edge or domain boundary is shown in Fig. 1a–b for better clarity.

An additional crystalline model was explored (Fig. 1d) to investigate the effect of randomness in domain sizes on basal plane thermal transport in MoS_2. In this model, randomly sized crystalline domains were introduced by creating 6 sharp interfaces from two 39 and 78 nm slabs with average domain sizes of ∼6.5 and ∼13 nm and with min/max domain sizes of 4/7.5 nm and 8/15 nm, respectively. All simulations were performed using the LAMMPS MD package[27] with simulation parameters as discussed in ref. 26. A cutoff of 10 Å was used for van der Waals and short range electrostatic interactions while long range electrostatics were modeled using PPPM methodology as implemented in LAMMPS. A time step of 1 fs was used for all MD simulations. Prior to thermal transport simulations, all systems were equilibrated using 200 ps of NVT simulations (canonical ensemble) at 300 K, followed by 200 ps of NPT simulations (isobaric ensemble) at 1 atmosphere pressure.

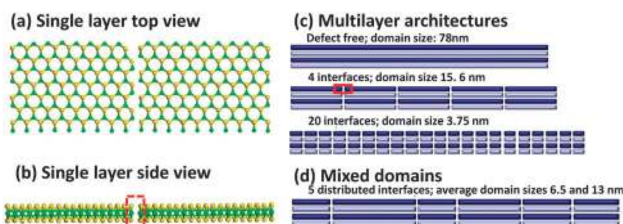

Fig. 1 (a) Top view and (b) side view representation of an edge-terminated domain boundary in a single MoS_2 layer. (c) Structures with a thickness of 4 monolayers with domains over a range of 4–78 nm in length within a 78 nm long MoS_2 crystal were examined in this work. (d) Mixed domain sizes were also examined.

Thermal transport simulations

Non-equilibrium molecular dynamics (NEMD) simulations based on the Fourier law approach[28] were used to estimate the in-plane thermal conductivity of MoS_2 crystalline grains (as discussed above). After equilibrating the system at the desired temperature and pressure, one boundary (∼3 nm width) of the large aspect ratio slab was heated and kept at a desired high temperature T_{high} (hot thermostat at 350 K) while the other boundary was cooled and kept at a desired low temperature T_{low} (cold thermostat at 250 K). In order to keep the thermostated regions at their specified temperatures, energy was continuously added and taken away from the hot and cold regions during the course of the simulation, respectively. This resulted in a temperature gradient across the slab. For calculating the steady state temperature profile, the elongated slab was divided into either 50 (for ∼39 nm long systems) or 100 (for ∼78 nm long system) thin slabs of equal thickness. Then, the temperature of each bin was calculated as follows:

$$T_i = \frac{1}{3N_i k_B}\sum_{k=1}^{N_i} m_k {v_k}^2$$

where, N_i is number of atoms in ith slab; and m_k and v_k correspond to atomic mass and velocity of atom k, respectively. Furthermore, the calculated temperature for each slab, T_i, was averaged over a pre-defined time interval to obtain a smooth temperature profile. Finally, the temperature gradient is calculated by the slope of the resulting temperature profile.

Similarly, heat flux per unit area, $Q/A\Delta t$, is calculated as follows:

$$\frac{Q}{A\Delta t} = \frac{1}{A\Delta t}\left\langle \frac{1}{2}\sum_{k=1}^{N_B} m_k\left({v_k}^2 - {vp_k}^2\right)\right\rangle$$

where, vp_k and v_k are the velocities of the atoms before and after rescaling to the desired temperature, respectively. N_B is the number of atoms in the boundary layers. Once the temperature gradient and the heat flux are known, thermal conductivity is calculated in a straightforward manner using Fourier's Law.

Results and discussion

Structure orientation control of deposited films

Fig. 2a shows a semi-log plot with examples of raw X-ray diffraction data from MoS_2 samples processed using different conditions of power modulation to highlight the accessible range of the (002) and (100) diffraction peak intensities.

 This journal is © the Owner Societies 2014

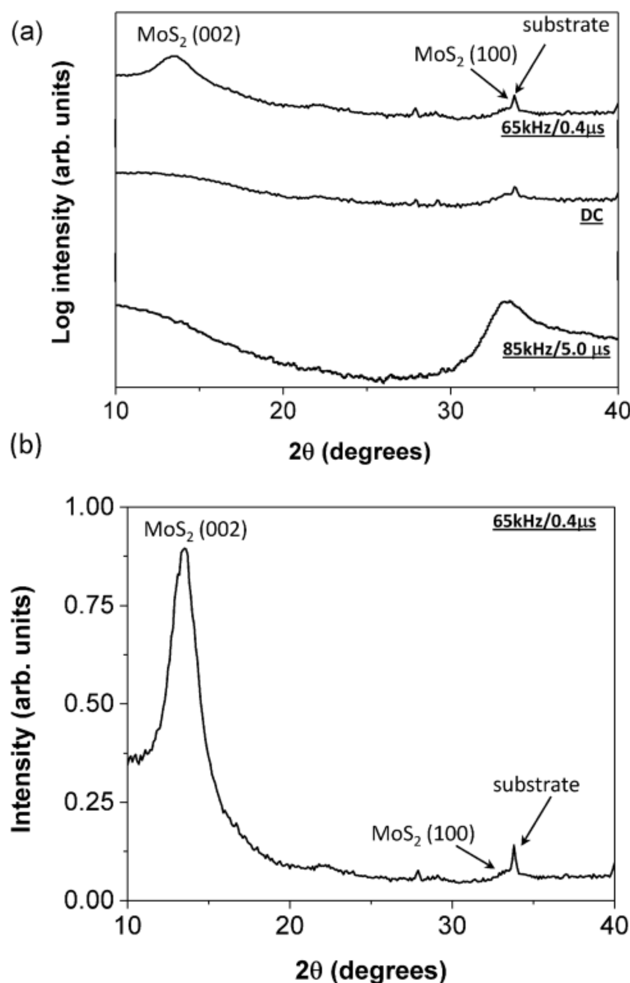

Fig. 2 (a) A semi-log plot of X-ray intensity for different sputtering power conditions (labeled in terms of pulse frequency and duration of positive pulse, or cathode off-time) depicting different orientations of 50 nm thin films. (b) Linear plot of example diffraction data for the 50 nm MoS_2 sample with the strongest (002) orientation. Note that the sharp peak overlapping with the broader MoS_2 (100) peak at 2θ = 33.8° is from the Inconel 718 substrate.

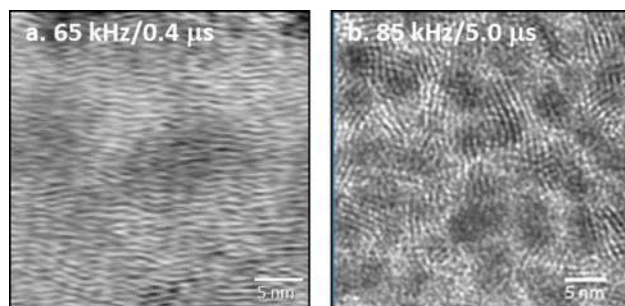

Fig. 3 TEM cross-sectional images from (a) strongly (002) oriented 50 nm sputtered MoS_2 film and (b) strongly (100) oriented MoS_2 film. Both images show a representative cross-sectional area observed close to surface of the film.

The highest and lowest (002)/(100) crystallographic ratios shown in Fig. 2a were obtained by adjusting the pulse parameters on the power supply as described in ref. 21. As an example, Fig. 2b shows a Bragg–Brentano diffractogram from the 50 nm film sputtered at 'high-rate' conditions (approximately 1 atomic layer per second) of 65 kHz with a 0.4 microsecond reverse time, yielding a film with strong (002) orientation. The strong (100) orientation was achieved under identical conditions, only with power modulation at 85 kHz with 5.0 microsecond reverse time. In all cases, the broadness of the MoS_2 peaks is related not only to domain size, but is also attributed to the expansion and contraction of the lattice due to atomic defects.[29]

It is evident from Fig. 2a, that the pulse characteristics have a strong effect on the orientation of the films. These parameters determine the arrival rate of the incident ions and atoms on the growing film, as well as their kinetic energy during film growth. Both of these factors can be used to obtain preferred orientation of MoS_2 films. Deposition rates of approximately 1 atomic layer per second (65 kHz/0.4 μs) yield the highest (002)/(001) ratios in the range of experimental parameters examined in this study. Promotion of growth on inert (002) basal plane surfaces is attributed to burial of atoms prior to desorption, which is estimated to be on the order of 1 second at 300 °C and under the conditions used in this work. Slower deposition rates inhibit (002) growth because most atoms incident on these surfaces are desorbed, promoting growth of the (100) orientation. Slower deposition rates can also increase the concentration of contaminant atoms, since the flux of Mo and S atoms is reduced in comparison to the flux from the ambient atmosphere in the processing chamber. A small atomic percent of contaminant atoms can disrupt (002) growth by exposing (100) plane edges to incident atomic fluxes. These planes grow at much higher rates in vapor phase growth processes due to reactive, exposed basal plane edges. Rapid growth of (100) oriented crystals can overshadow the slow-growing (002) planes[22] leading to preferred (100) orientation. Given the low base pressure in the current studies, we presume that the desorption phenomena primarily dictate orientation, as contaminant fluxes are low during growth. We also produced an X-ray amorphous MoS_2 thin film by DC sputtering on a room temperature substrate. Consistent with the literature on sputtered MoS_2, the low ion flux and relatively low kinetic energy typical of dc sputtering[21] coupled with low atomic mobility at room temperature result in amorphous MoS_2 thin films.[30,31]

Fig. 3 shows cross-sectional TEM micrographs of the 150 nm thick film surface with preferred (a) (002) growth and (b) (100) growth, corresponding to the high-rate (65 kHz/0.4 μs reverse time) and low-rate (85 kHz/5.0 ms reverse time) magnetron sputtered films, respectively, as called out in Fig. 2. The images are taken near the surface of the film, but are representative of the homogeneous microstructure observed throughout the film thickness. Analysis of the TEM images from Fig. 3 suggests the average crystalline domain sizes on the order of ~5 nm in the deposited films. Preparation of samples by focused ion beam milling and cross-sectional electron microscopy was completed for each sample to determine thickness, and all samples were within 10% of the nominal thickness.

Effect of environmental humidity on layer composition

X-ray photoelectron spectroscopy (XPS) was used to examine and compare the compositions of as-deposited and exposed

View Article Online

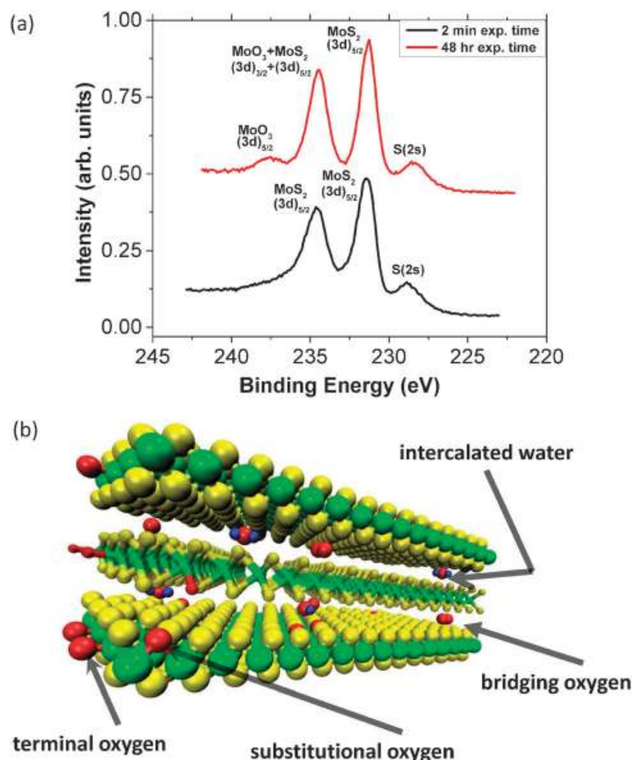

Fig. 4 (a) High resolution scans of molybdenum 3d X-ray photo electron spectroscopy peaks for 100 nm MoS_2 samples characterized immediately after removal from the processing chamber (black curve); and measured after 48 hours of exposure to laboratory air with approximately 35% relative humidity (red curve). A schematic diagram showing possible oxygen or water ingress locations within the MoS_2 crystal is shown in (b).

films (to humid air for 48 hours). Fig. 4a shows the high resolution scans of the Mo (3d) peaks arising from its oxidation states in deposited films subjected to different durations of exposure to environmental humidity. The sample with no exposure to air (black) shows only a Mo doublet (Mo^{4+} oxidation state) and an S (2s) peak (S^{2-} oxidation state) which are characteristic of MoS_2. However, the shoulder at higher binding energy for the 48 hour exposed sample (red) is clearly indicative of MoO_3 formation (another doublet in which the lower energy peak of MoO_3 overlaps with higher energy peak of MoS_2 doublet, giving rise to a three Mo peak structure),[32,33] due to oxygen ingress on exposure to the humid ambient environment. Fig. 4b schematically shows three possible ways in which oxygen can be integrated into MoS_2 films which are described in the literature—as substitutional atoms at sulfur sites,[34] as atoms bound to molybdenum atoms at plane edges,[32] or as an intercalant between basal planes as O_2 or moisture (H_2O).[35] We believe that the Mo (3d) peak structure shown in Fig. 4a (red curve) results from edge plane termination by oxygen *via* diffusion at domain boundaries. This type of oxygen incorporation, is expected to occur after deposited film exposure to humid atmosphere, while oxygen substitution is generally introduced during film growth.[32] We observed no oxygen in these materials immediately after growth with the *in vacuo* XPS experiments, indicating that oxygen concentrations in the materials are less than 1 atomic percent. Examination of the X-ray diffraction peaks in Fig. 2 could yield evidence of intercalation, however fork and splitting defects within the MoS_2 result in broad diffraction peaks which may obscure a shifted portion of the (002) diffraction peak.[11] We cannot determine from our data if intercalation is a mechanism of water or oxygen ingress, however the Mo–O peak observed *via* XPS is strong evidence of edge terminated and diffused oxygen at domain boundaries.

Thermal conductivity – experimental measurement

Thermal conductivity values for a series of amorphous and ordered MoS_2 films of different thicknesses, as measured from TDTR technique, are shown on Fig. 5. For all samples studied, TDTR data were acquired from 10 locations on each sample surface. The scans were individually modeled, and an average thermal conductivity value was calculated for each sample. For MoS_2 surfaces coated in an UHV environment with the Al transducer material immediately after growth (*i.e.*, no exposure to the ambient environment), we observe that the thermal conductivity was essentially independent of thickness from 50–150 nm (compared to error bars), and varied from 0.25 to 1.5 W m^{-1} K^{-1} for the (002) and (100) orientations, respectively. Thermal conductivity of a geological MoS_2 specimen along the (002) direction was also measured *via* the TDTR technique to be approximately 3.0 W m^{-1} K^{-1}. The conductivity values for (002) oriented thin films are over a factor of 10 lower than those measured for the bulk crystal, and a factor of three lower than those measured for the amorphous films. This reduction is due to the scattering at domain boundaries that dominates phonon conduction in nanostructured TMD films.[11,18] Interestingly, (002) oriented films subjected to atmospheric exposure ($\sim$48 hours) prior to application of the transducer layer were measured to have a thermal conductivity of $\sim$1.0 W m^{-1} K^{-1}, while maintaining their (002) orientation. This is approximately 4 times higher than unexposed MoS_2 films along (002) orientation and

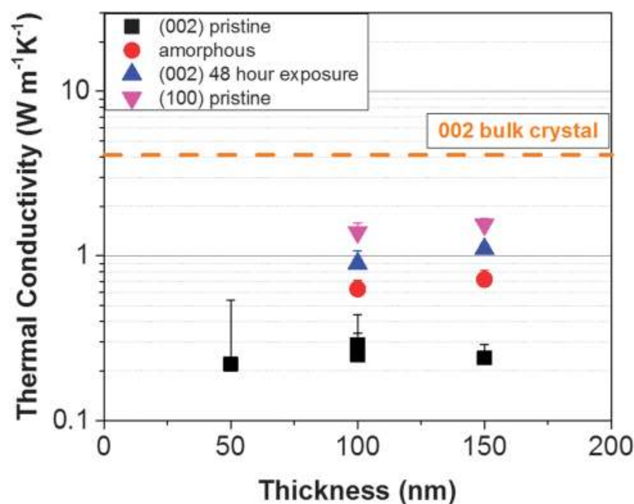

Fig. 5 Plot of thermal conductivity measured for MoS_2 with different thicknesses and microstructures as denoted. The (002) plane bulk thermal conductivity of the geological specimen is also shown.

This journal is © the Owner Societies 2014

close to the values measured for films with (001) orientation, demonstrating that the thermal conductivity of the (002) oriented films is strongly dependent upon their atmospheric exposure history. It is expected that MoS_2 materials with fewer domain boundaries (resulting in fewer exposed plane edges) would possess a reduced environmental sensitivity. We propose that the observed increase in thermal conductivity with extended exposure to humid air and subsequent MoO_3 formation is likely due to bridging of van der Waals gaps between MoS_2 layers by stiffer bonds at edges throughout the thickness of the film materials, increasing the thermal energy exchange across domain boundary interfaces *via* more strongly bonded interactions. A similar environmental sensitivity can expected for mono- and few-layer MoS_2 films, indicating that maximizing grain size will be important for stability of thermal and perhaps other properties of the materials.

Thermal conductivity – predictions from simulations

The in-plane thermal conductivity of the oriented crystalline domains (schematically shown in Fig. 1c, d) was calculated using NEMD simulations and is plotted in Fig. 6. In order to place the predicted values in a broader perspective, we compare our simulation results for the pristine MoS_2 case with published experimental data prior to a discussion of effects of nano-crystallinity, *i.e.*, the effect of crystalline domains on thermal conduction in MoS_2 thin films. In this context, Fig. 6 shows the thermal conductivity of a $\sim$70 nm pristine slab (no defects) to be $\sim$44 W m^{-1} K^{-1}. Using the same force field, we previously predicted the thermal conductivity of a shorter $\sim$20 nm pristine slab to be $\sim$18 W m^{-1} K^{-1},[26] suggesting a notable length dependence on in-plane thermal conductivity similar to that of pristine graphite/graphene at such length scales.[16] Recently, based on experimental Raman data, Sahoo *et al.* also predicted the in-plane thermal conductivity of high-quality few-layer (11 layers) MoS_2 films to be $\sim$52 W m^{-1} K^{-1}.[12] It is interesting to note the compelling agreement in predicted thermal conductivity values of defect free MoS_2 with two entirely different methods. The origin of this similarity can be attributed to the fact that vibrational characteristics of MoS_2 were exploited to predict the values in both approaches. With regards to cross-plane thermal conduction, our previously reported value of $\sim$4 W m^{-1} K^{-1} (ref. 26) for defect-free MoS_2 is also in good agreement with current experimental data obtained from a bulk (002) oriented geological specimen ($\sim$3.0 W m^{-1} K^{-1} in Fig. 5). Lastly, we should point out that the thermal anisotropy factor of $\sim$15–20 for 'pristine' MoS_2 is also in accordance with other TMD materials such as WSe_2.[20]

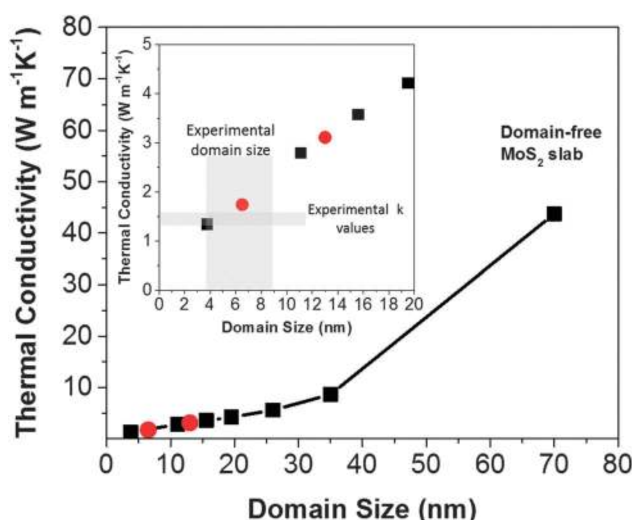

Fig. 6 Simulated in-plane thermal conductivity values of MoS_2 comprised of identical (black squares) and distributed (red circles) domain lengths. The inset zooms in on lower domain size results and compares the results with experimentally measured value of thermal conductivity for MoS_2 along in-plane direction, as represented by shaded region.

It is imperative to understand the mechanism of reduced in-plane MoS_2 thermal conductivity for nanocrystalline films in comparison to its bulk-like morphology,[12] with the primary difference between the two being the nature and density of defects within the material. While point defects are known to impact thermal conductivity,[36] the magnitude of the impact is related to the concentration of defects and the mass difference between the defect atom and the atom it replaces. Oxygen substitution for sulfur, as discussed previously, would be the point defect with highest concentration, however the oxygen concentration in films immediately capped with Al was undetectable with XPS. The primary difference is therefore the high density of domain boundaries throughout the thickness (Fig. 3) which increases as the domain size shrinks. Fig. 6 showcases this very issue and highlights the sharp drop in effective in-plane thermal conductivity of MoS_2 with reduction in nano-crystalline domain size. For the smallest studied 'identical' crystalline domains of $\sim$4 nm, a thermal conductivity of $\sim$1.3 W m^{-1} K^{-1} was predicted. The figure also plots the predicted in-plane thermal conductivity of studied 'distributed' parallel crystalline domains with two different average sizes of 6.5 and 13 nm. As seen from the inset more clearly, the predicted values for 'distributed' domains match the homogeneous 'identical size' crystalline domains. The Fig. 6 inset also compares the measured thermal conductivity of deposited MoS_2 film along the (100) direction with those of predicted by simulations. For $\sim$5 nm crystalline domains (along with its approximate distribution as shown in Fig. 3), the simulation prediction ($\sim$1.5 W m^{-1} K^{-1}) matches well with that of experimental measurement ($\sim$1.1 W m^{-1} K^{-1}). Overall, a strong thermal conductivity dependence on the size of crystalline domains, predicted by simulations and confirmed by experiments, clearly demonstrates the significance of thermal boundary scattering at the sharp interfaces limiting thermal conduction in nano-crystalline thin film MoS_2. Our observation of thickness independence of thermal conduction in thin films also indicates that the overall thermal conductivity of the films is dominated/limited by the domain sizes of the nano-crystalline MoS_2. For completeness, we should point out that incorporation of oxygen and hydrogen in simulations would require further parameterization and validation of the updated force field to build upon the approach discussed in the present study.

Conclusions

Thin films of MoS_2 with strong (002) and (100) orientations were grown to thicknesses of 50–150 nm. Thermal conductivity was measured for both orientations at incremental thicknesses and was found to be approximately 1.5 W m^{-1} K^{-1} along MoS_2 basal planes compared to 0.25 W m^{-1} K^{-1} across the basal planes for samples that were not exposed to ambient air. Cross-plane thermal conductivity measurement of a bulk geological MoS_2 crystal revealed a thermal conductivity >10 times higher than that of the film materials, suggesting the significant role of defects arising from the films' turbostratic structure. We observed that environmental sensitivity of the (002) oriented MoS_2 films exposed to humid air was manifested as a 4 fold increase in cross-plane thermal conductivity. The MD simulations of thermal conduction in perfect (100) MoS_2 crystals and those with a range of defect densities demonstrated a significant reduction in conductivity with incorporation of relatively low defect densities. The predicted thermal conductivity values correlated well to experimental observations, confirming the role of thermal boundary scattering as dominating mechanisms in limiting thermal conductivity in nano-crystalline thin films of MoS_2.

Acknowledgements

This research was sponsored by the Air Force Office of Scientific Research, Thermal Sciences Program. CM thanks Advanced Energy Industries Inc. for providing a power supply used for materials processing. The authors also thank Prof. D.G. Cahill, Prof. W.P. King and their former student Ryan McLaren at the University of Illinois Urbana-Champaign and T.S. Fisher at Purdue University for insightful discussions and collaborative efforts associated with this work.

References

1 W. E. Jamison and S. L. Cosgrove, *ASLE Trans.*, 1971, **14**, 62–72.
2 R. Chianelli, M. H. Siadati, M. P. De La Rosa, G. Berhault, J. P. Wilcoxon, R. Bearden and B. L. Abrams, *Catal. Rev.*, 2006, **48**, 1.
3 K. F. Mak, C. Lee, J. Hone, J. Shan and T. F. Heinz, *Phys. Rev. Lett.*, 2010, **105**, 136805.
4 D. G. Cahill, W. K. Ford, K. E. Goodson, G. D. Mahan, A. Majumdar, H. J. Maris, R. Merlin and S. R. Philpot, *J. Appl. Phys.*, 2003, **93**, 793.
5 Q. H. Wang, K. Kalantar-Zadeh, A. Kis, J. N. Coleman and M. S. Stano, *Nat. Nanotechnol.*, 2012, **7**, 699.
6 M. P. Levendorf, C.-J. Kim, L. Brown, P. Y. Huang, R. W. Havener, D. A. Muller and J. Park, *Nature*, 2012, **488**, 627.
7 R. Fivaz and E. Mooser, *Phys. Rev.*, 1967, **163**, 743.
8 F. K. Perkins, A. L. Friedman, E. Cobas, P. M. Campbell, G. G. Jernigan and B. T. Jonker, *Nano Lett.*, 2013, **13**, 668–673.
9 J. Feng, X. Qian, C.-W. Huang and J. Li, *Nat. Photonics*, 2012, **6**, 866.
10 S. Bertolazzi, J. Brivio and A. Kis, *ACS Nano*, 2011, **12**, 9703.
11 C. Muratore, V. Varshney, J. J. Gengler, J. J. Hu, J. E. Bultman, T. M. Smith, P. J. Shamberger, B. Qiu, X. Ruan, A. K. Roy and A. A. Voevodin, *Appl. Phys. Lett.*, 2013, **101**, 081604.
12 S. Sahoo, A. P. S. Gaur, M. Ahmadi, M. J.-F. Guinel and R. S. Katiyar, *J. Phys. Chem. C*, 2013, **117**, 9042.
13 C. A. Klein and M. G. Holland, *Phys. Rev.*, 1964, **136**, a575.
14 G. A. Slack, *Phys. Rev.*, 1962, **127**, 694–701.
15 E. K. Sichel, R. E. Miller, M. S. Abrahams and C. J. Buiocchi, *Phys. Rev. B: Solid State*, 1976, **13**, 4607.
16 E. Pop, V. Varshney and A. K. Roy, *MRS Bull.*, 2012, **37**, 1.
17 I. Jo, M. T. Pettes, J. Kim, K. Watanabe, T. Tanigucki, Z. Yao and L. Shi, *Nano Lett.*, 2013, **13**, 550.
18 C. Chiritescu, D. G. Cahill, N. Nguyen, D. C. Johnson, A. Bodapati, P. Keblinski and P. Zschack, *Science*, 2007, **315**, 351.
19 N. T. Nguyen, P. A. Berseth, Q. Lin, C. Chiritescu, D. G. Cahill, A. Mavrokefalos, L. Shi, P. Zschack, M. D. Anderson, I. M. Anderson and D. C. Johnson, *Chem. Mater.*, 2010, **22**, 2750.
20 A. Mavrokefalos, N. T. Nguyen, M. T. Pettes, D. C. Johnson and L. Shi, *Appl. Phys. Lett.*, 2007, **91**, 171912.
21 C. Muratore and A. A. Voevodin, *Thin Solid Films*, 2009, **517**, 5605.
22 J. Moser and F. Levy, *J. Mater. Res.*, 1993, **8**, 206.
23 D. G. Cahill, *Rev. Sci. Instrum.*, 2004, **75**, 5119.
24 J. J. Gengler, C. Muratore, A. K. Roy, J. J. Hu, A. A. Voevodin, S. Roy and J. R. Gord, *Compos. Sci. Technol.*, 2010, **14**, 2117.
25 T. Hupf, C. Cagran, E. Kaschnitz and G. Pottlacheer, *Thermochim. Acta*, 2009, **494**, 40.
26 V. Varshney, S. S. Patnaik, C. Muratore, A. K. Roy, A. A. Voevodin and B. L. Farmer, *Comput. Mater. Sci.*, 2010, **48**, 101.
27 S. Plimpton, *J. Comput. Phys.*, 1995, **117**, 1.
28 A. J. H. McGaughey and M. Kaviany, *Adv. Heat Transfer*, 2006, **39**, 169.
29 D. N. Dunn, L. E. Seitzman and I. L. Singer, *J. Mater. Res.*, 1997, **12**, 1191.
30 T. Spalvins, *Thin Solid Films*, 1980, **73**, 291.
31 B. C. Stupp, *Thin Solid Films*, 1981, **84**, 257.
32 P. D. Fleischauer and J. R. Lince, *Tribol. Int.*, 1999, **32**, 627.
33 N. M. D. Brown, N. Cui and A. McKinley, *Appl. Surf. Sci.*, 1998, **134**, 11.
34 J. R. Lince, M. R. Hilton and A. S. Bommannavar, *Surf. Coat. Technol.*, 1990, **43/44**, 640.
35 X. Zhao and S. S. Perry, *ACS Appl. Mater. Interfaces*, 2010, **2**, 1444.
36 P. G. Klemens, *Phys. Rev.*, 1960, **119**, 507.

This journal is © the Owner Societies 2014